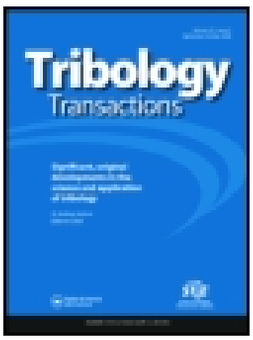

Tribology Transactions

ISSN: 1040-2004 (Print) 1547-397X (Online) Journal homepage: http://www.tandfonline.com/loi/utrb20

New EHL Modeling Data for the Reference Liquids Squalane and Squalane Plus Polyisoprene

Scott S. Bair, Ove Andersson, Farrukh S. Qureshi & Michele M. Schirru

To cite this article: Scott S. Bair, Ove Andersson, Farrukh S. Qureshi & Michele M. Schirru (2017): New EHL Modeling Data for the Reference Liquids Squalane and Squalane Plus Polyisoprene, Tribology Transactions, DOI: 10.1080/10402004.2017.1310339

To link to this article: http://dx.doi.org/10.1080/10402004.2017.1310339

Accepted author version posted online: 27 Mar 2017.
Published online: 27 Mar 2017.

TRIBOLOGY TRANSACTIONS
http://dx.doi.org/10.1080/10402004.2017.1310339

stle
Society of Tribologists and Lubrication Engineers

New EHL Modeling Data for the Reference Liquids Squalane and Squalane Plus Polyisoprene

Scott S. Bair[a], Ove Andersson[b], Farrukh S. Qureshi[c], and Michele M. Schirru[d]

[a]Georgia Institute of Technology, Center for High-Pressure Rheology, George W. Woodruff School of Mechanical Engineering, Atlanta, Georgia; [b]Department of Physics, Umeå University, Umeå, Sweden; [c]Applied Sciences, The Lubrizol Corporation, Wickliffe, OH, USA; [d]Leonardo Centre for Tribology, Department of Mechanical Engineering, University of Sheffield, Sheffield, United Kingdom

ABSTRACT

An important part of the new quantitative approach to elastohydrodynamic lubrication (EHL) is the use of reference liquids with well-characterized thermophysical properties. New measurements are reported for the thermal and rheological properties of squalane to high pressure and of high shear rate and high-frequency viscosity of squalane thickened with polyisoprene (SQL + PIP) at ambient pressure. The glass transition viscosity of squalane at ambient pressure was found from published viscosity measurements and new glass transition measurements by transient hot wire. The glass transition viscosity so determined was incorporated into the improved Yasutomi model and the calculated glass transition temperatures as a function of pressure are comparable to those directly measured, although the hybrid model yields better agreement. The glass transition viscosity of squalane by any definition must be substantially lower than the "universal value" of 10^{12} Pa·s. The second Newtonian inflection cannot be characterized in steady shear at ambient pressure for SQL + PIP due to cavitation; however, acoustic viscometry with matching layer does characterize the second Newtonian inflection. To form the analogy between steady and oscillatory shear requires that the steady shear rate be compared with the ordinary frequency rather than the angular frequency for SQL + PIP.

ARTICLE HISTORY
Received 29 December 2016
Accepted 17 March 2017

KEYWORDS
Quantitative elastohydrodynamics; high-pressure rheology; high-shear viscosity; reference liquids

Introduction

When liquid lubricants are entrained in the contact between nonconformal solids of high yield strength and elastic modulus, the liquid film must necessarily be compressed to high pressure. The liquid responds to the pressure with greatly increased viscosity. These elastohydrodynamically lubricated contacts, in contrast to hydrodynamically lubricated contacts, are small and easily isolated to study film thickness and friction. It should therefore be expected that, over time, the mechanisms of film formation and friction would be thoroughly revealed through experiment and analysis. This has not occurred.

The field of elastohydrodynamic lubrication (EHL) has an unusual history. It is one of the few fields that requires a knowledge of the thermophysical properties of liquids at high pressures, above 0.5 GPa. Despite significant progress in measurement techniques at high pressures (Holzapfel and Isaacs *(1)*) over the last 40 years, EHL has resisted the use of accurate properties in analysis, although the situation has improved significantly since the mid-1990s when viscosity measurements at high pressure were effectively banned by the peer review process. As an example, in EHL, liquid compressibility is given by the Hayward *(2)* equation (known in EHL as Dowson and Higginson) with a compression limit and parameters that do not vary with temperature or the type of liquid; Hayward *(2)* found that this expression was accurate to only 0.1 GPa and then with the appropriate parameterization. By far the most egregiously misrepresented property has been viscosity. Comparisons of viscometer measurements with the viscosity employed in EHL analyses began more than 40 years ago with the significant work of Hutton and Phillips *(3)*. They found orders of magnitude error in the viscosity used in an analysis of transient EHL entrapment. It has been an accepted technique within EHL to adjust viscosity to reach agreement with experimental results, and this procedure continues today (Bair *(4)*; Bair, et al. *(5)*, *(6)*).

As a result of the acceptance and use of adjusted viscosities, this field has been unable to demonstrate that false assumptions are, in fact, false. One of these false assumptions has been the Newtonian inlet zone. Only recently have methods been developed to account for film thickness with shear-dependent viscosity (Habchi, et al. *(7)*), and one of the reference liquids used to validate the method, squalane plus polyisoprene (SQL + PIP), is the subject of this article.

Another related false assumption is that the logarithmic shape of a friction curve results from the logarithmic dependence of shear stress on shear rate; that is, the Eyring sinh law (Ree, et al. *(8)*). An excellent example is the work of Johnson and Tevarrwerk *(9)*. Although the pressure dependence of

CONTACT Scott S. Bair scott.bair@me.gatech.edu

Color versions of one or more of the figures in the article can be found online at www.tandfonline.com/utrb.

Review led by Guillermo Morales Espejel.

Nomenclature

$A_1, A_2, b_1, b_2, C_1, C_2$ = Yasutomi parameters (various units)
a = Yasuda parameter
C_p = Heat capacity (J/kg·K)
D_F = Fragility parameter
F = Relative thermal expansivity of the free volume
f = Normal frequency (Hz)
G = Stress at the intersection of the terminal and power law regimes (Pa)
M = Molecular mass (kg/kmol)
m = Shifting exponent
N_1 = Primary normal stress difference (Pa)
n = Power law exponent
p = Pressure (Pa)
q = McEwen exponent
R_g = Universal gas constant (8,314 J/kmol·K)
T = Temperature (K)
T_∞ = Divergence temperature (K)
T_g = Glass transition temperature (K or°C)
T_{g0} = Glass transition temperature at $p = 0$ (K or°C)
α_0 = Initial pressure–viscosity coefficient (Pa^{-1})
$\dot{\gamma}$ = Shear rate (s^{-1})
η = Rate-dependent steady shear viscosity (Pa·s)
$\hat{\eta}$ = Frequency dependent oscillatory shear viscosity (Pa·s)
κ = Thermal conductivity (W/m·K)
λ_{diel} = Dielectric relaxation time (s)
λ_{Cp} = Heat capacity relaxation time (s)
μ = Limiting low-shear viscosity (Pa·s)
μ_0 = Low-shear viscosity at $p = 0$ (Pa·s)
μ_∞ = Low-shear viscosity for zero argument of the exponential (Pa·s)
ρ = Mass density (kg/m^3)
τ = Shear stress (Pa)
ω = Angular frequency (rad/s)

viscosity is unlike any measured in a viscometer, this article has had a profound influence on EHL and is the basis of the non-Newtonian model most often applied to high-pressure EHL films, although it has not been applied using accurate pressure dependence of viscosity.

The assumption that a logarithmic friction response results from a logarithmic constitutive response can be tested with one of the reference liquids that are the subject of this article. Squalane (SQL) was employed for a full thermal EHL simulation of friction (Björling, et al. *(10)*) over a wide range of operating parameters using models for the temperature, pressure, and shear dependence of viscosity derived from viscometer measurements and models for the temperature and pressure dependence of the thermal properties derived from hot-wire measurements. Traction (friction) curves were generated and, for one to two decades of slide-to-roll ratio, the friction varied as the logarithm of sliding velocity. The calculations were experimentally validated (Björling, et al. *(10)*). In Fig. 1, the calculated logarithmic response is shown for a Hertzian pressure of 1.07 GPa and temperature of 40°C. The straight line indicates a slope; that is, an "Eyring stress," of 9.3 MPa. However, the shear dependence of viscosity for the calculation was power law (Björling, et al. *(10)*), not sinh law. The logarithmic friction disappears when the stress limit is removed, as shown in Fig. 1. Therefore, the logarithmic friction response of squalane results from super-Arrhenius piezoviscosity and a pressure-proportional stress limit (Bair, et al. *(11)*), not a logarithmic constitutive response.

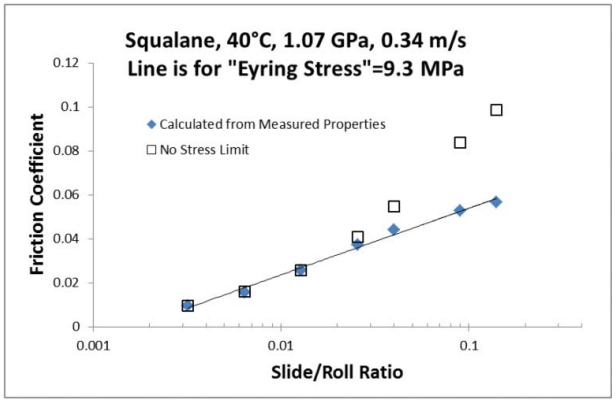

Figure 1. Friction coefficient calculated in Björling, et al. *(10)* showing that a logarithmic response requires a stress limit.

An alternative to the classical approach of EHL appeared about 10 years ago. Quantitative EHL (Bair, et al. *(12)*) employs real, measureable thermophysical properties of the liquid, in contrast to classical EHL, which employs fictional narratives concerning the works of Barus, Roelands, and Eyring to adjust these properties to suit the purpose at hand. Reference liquids with well-characterized thermophysical properties at the pressures of EHL have been an important part of the new quantitative elastohydrodynamics.

One such reference liquid is squalane, 2,6,10,15,19,23-hexamethyltetracosane, which has pressure-dependent viscosity similar to a 4 cSt polyalphaolefin (Bair *(13)*). It was obtained from a chemical supply house with stated purity of 99%. This liquid was used by Liu and coworkers *(14)* in the first numerical solution for EHL film thickness to employ real viscosity and the agreement with experimental film thickness by colorimetric interferometry was striking. The description of the pressure dependence employed by Liu and coworkers *(14)* was in sharp contrast to the pressure–viscosity coefficient of squalane required to explain the thickness of thin films by classical EHL (Johnston, et al. *(15)*), which bears no relation to primary measurements. New discoveries followed rapidly once it was demonstrated that both film thickness and friction could be accurately explained and predicted (Björling, et al. *(10)*; Liu, et al. *(16)*; Krupka, et al. *(17)*, *(18)*; Habchi, et al. *(19)*) without adjusting the properties of the liquid. SQL has been an important subject for these EHL investigations and it was first suggested as a reference standard (Sax and Stross *(20)*) six decades ago.

Another reference liquid (SQL + PIP) is a solution of 15% by weight cis-polyisoprene (PIP) in squalane, intended to be representative of the polymer-blended multigrade gear oils and engine oils (Bair *(21)*). The PIP has molecular mass of 4×10^4 kg/kmol and one of the authors has stored 0.5 kg. Notably, this reference liquid was employed to validate an EHL film thickness formula for liquids displaying a second Newtonian viscosity inflection (Habchi, et al. *(7)*).

This article adds to the considerable existing literature (Bair *(4)*, *(13)*, *(21)*; Habchi, et al. *(7)*; Björling, et al. *(10)*; Sax and Stross *(20)*; Harris *(22)*; Pensado, et al. *(23)*; Fandino, et al. *(24)*; Comuñas, et al. *(25)*) some new additional high-pressure thermophysical property measurements on SQL along with correlations for SQL and for SQL + PIP from four different laboratories. For SQL, the thermal conductivity and heat capacity were measured to high pressure at Umeå University and the viscosity was measured to very high pressure at Georgia Tech. For SQL + PIP at ambient pressure, the viscosity at high shear rate was measured at Lubrizol and the viscosity at high frequency was measured at the University of Sheffield.

Squalane glass transition

Oddly, there is little mention of the glassy state in EHL literature, although many numerical simulations have treated the lubricant as if the liquid were at temperatures well below the glass transition temperature at the Hertzian pressure. Liquid lubricants readily supercool. That is, they avoid crystallization on cooling or compression and become solid only by vitrification. The viscosity becomes so large that no liquid-like response is possible and by most means of observation the material is solid. In contrast to crystallization, the glass transition occurs over a range of temperature or pressure, and for a given means of detecting the transition it occurs at a specific viscosity, μ_g, that is independent of temperature and pressure. Therefore, the glass transition point can be used as a marker for viscosity in EHL studies.

The Williams, Landel, and Ferry (WLF; Williams, et al. *(26)*) equation,

$$\mu = \mu_g \exp\left[\frac{-2.303C_1(T - T_g)}{C_2 + (T - T_g)}\right], \qquad [1]$$

is equivalent to the Vogel, Tammann, and Fulcher (VTF) equation (Angell *(27)*),

$$\mu = \mu_\infty \exp\left[\frac{D_F T_\infty}{T - T_\infty}\right]. \qquad [2]$$

The WLF and VTF equations are related by $D_F T_\infty = C_2 \ln(\mu_g/\mu_\infty)$, $\mu_g = \mu_\infty \exp(2.303C_1)$, and $T_\infty = T_g - C_2$. The WLF equation employs the glass transition as an isoviscous reference state and can be derived from the concept of free volume.

Yasutomi and coworkers *(28)* applied the WLF equation to both the temperature and the pressure dependence of viscosity by making the glass transition temperature, T_g, and the relative thermal expansivity of the free volume, F, functions of pressure:

$$\mu = \mu_g \exp\left[\frac{-2.303C_1(T - T_g(p))F(p)}{C_2 + (T - T_g(p))F(p)}\right] \qquad [3]$$

using the Oels and Rehage *(29)* equation for the glass transition pressure.

$$T_g(p) = T_{g0} + A_1 \ln(1 + A_2 p). \qquad [4]$$

There is an advantage in a correlation that employs the glass transition. The measurement of T_g as a function of pressure by dilatometry is relatively easy (Weitz and Wunderlich *(30)*) compared to viscometry at high pressures and the empirical function [4] is accurate for elevated pressure. Recently, an improved function for the pressure dependence of the relative thermal expansivity of the free volume, $F(p)$, was introduced (Bair, et al. *(31)*) to correct nonphysical behavior at high pressure:

$$F = (1 + b_1 p)^{b_2}. \qquad [5]$$

The fit at low pressure also improves with Eq. [5].

The thermal properties for elevated pressure of squalane; thermal conductivity, κ; and volumetric heat capacity, ρC_p, were required in a previous numerical simulation predicting friction in the thermoviscous regime of EHL traction (Björling, et al. *(10)*); empirical relations for the temperature and pressure dependence of the thermal conductivity and volumetric heat capacity may be found in Björling, et al. *(10)*. These properties were measured by the transient hot-wire method (Håkansson, et al. *(32)*). The glass transition was revealed in these measurements as shown in Figs. 2 and 3 for thermal conductivity and volumetric heat capacity, respectively. In particular, the heat capacity goes from a large liquid-like value to a relatively smaller solid-like value as the temperature is reduced. A peak in conductivity marks the transition. The glass transition temperatures are listed as a function of pressure in Table 1 and for ambient pressure, T_g = 174.4 K. Combining the uncertainties

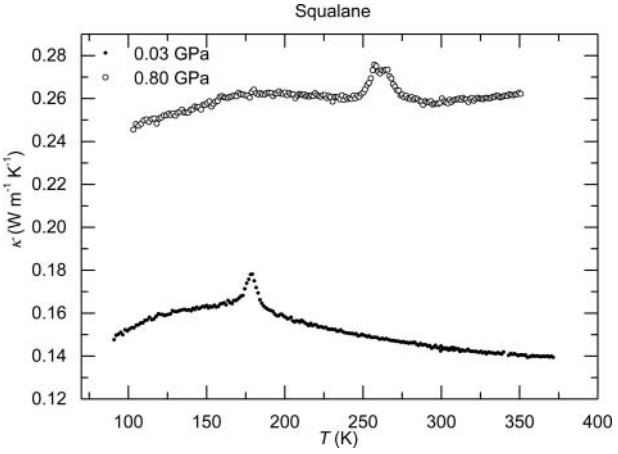

Figure 2. Temperature dependence of the thermal conductivity of squalane at pressures of 30 and 800 MPa.

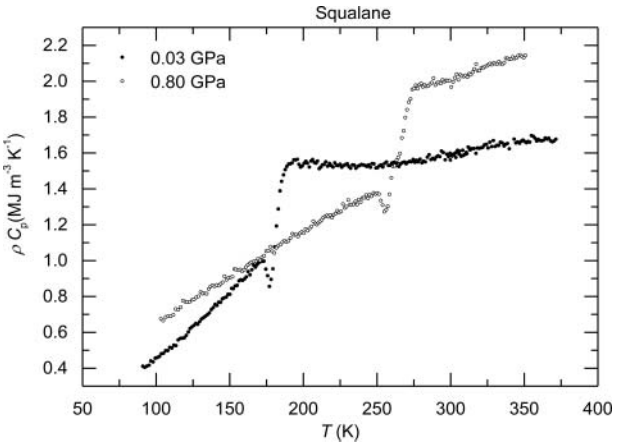

Figure 3. Temperature dependence of the volumetric heat capacity of squalane at pressures of 30 and 800 MPa.

in temperature and pressure gives an estimated uncertainty in T_g of 1 K. Fitting the Oels and Rehage *(29)* equation gives $A_1 = 200$ K and $A_2 = 0.650$ GPa^{-1}. The measurement of a glass transition temperature is associated with a characteristic time of the experiment. Because of the short characteristic time of the hot-wire experiment, the heat capacity relaxation time is only about $\lambda_{Cp} = 0.3$ s (Andersson *(33)*) at the glass transition temperature in Figs. 2 and 3.

Squalane viscosity

The viscosity at the glass transition, μ_g, has been the subject of speculation, and given the extreme difficulty in measuring this property it is ordinary assigned an estimated "universal" value of 10^{12} Pa·s. Matusita and coworkers *(34)* found that for three fluoride glasses in isobaric cooling, μ_g increases with decreasing cooling rate and that 10^{12} Pa·s was the value for all glasses studied in the limit of zero rate. Giordano, et al. *(35)* found $\mu_g = 10^{11.09}$ Pa·s for volcanic minerals. Schweyer *(36)* found $\mu_g = 10^8$ Pa·s for asphalts under pressure. Bair *(37)* required $\mu_g = 10^{9.1}$ Pa·s to fit the original Yasutomi model to viscosity and glass transition measurements on a naphthenic mineral oil. In the original formulation of the Yasutomi model, it was sometimes necessary to assume μ_g to be as low as 10^7 Pa·s to be consistent with dilatometer measurements of $T_g(p)$ (Yasutomi, et al. *(28)*). In tribology, the glass transition of oils has traditionally been studied by dilatometry or light scattering (Alsaad, et al. *(38)*).

Table 2. New viscosity measurements (Pa·s) for squalane at indicated temperatures and pressures.

	Pa s	
p (MPa)	21.5°C	40°C
1,000	20,000	
1,100	75,000	
1,200	350,000	13,000
1,300		44,000
1,350		91,000

Deegan and coworkers *(39)* have presented viscosity measurements of squalane at ambient pressure down to 169 K that cross the glass transition. Their data were successfully fitted to a single VTF equation (Eq. [2]; Deegan, et al. *(39)*), thus precluding a dynamic crossover. Solving for $T = 174.4$ K gives the glass viscosity as $\mu_g = 1.23 \times 10^7$ Pa·s ($10^{7.09}$ Pa·s) for squalane. This value for the glass viscosity can be incorporated into the improved Yasutomi model (Hutton and Phillips *(3)*). For this purpose, viscosities are available from Bair *(21)* for pressure to 1.0 GPa at 20°C and to 1.2 GPa at 40 and 65°C. The estimated uncertainty is 4%. To generate viscosity data closer to the glass pressure at more usual EHL temperatures, additional viscosity measurements were performed in a falling cylinder viscometer.

The viscometer is an improved version of the instrument described in Bair *(40)*. The intensifier pressure relation is now determined by the resistance of a manganin wire that was calibrated with a dead-weight tester to 1.4 GPa. The hollow sinker was fabricated with an iridium core. The large mass density of iridium reduces the error in the buoyancy correction resulting from error in the sample density estimate. Density was estimated from the Tait equation (Bair *(21)*). Measurements were made at 21.5 and 40°C. It was not possible to repeat the previous results at 20°C because of the high laboratory ambient temperature of an Atlanta summer. The new measurements are reported in Table 2. Because of the rather long fall times, lasting up to 4 h, the estimated uncertainty in viscosity is 12% here. Uncertainties for pressure and temperature are 5 MPa and 0.3°C, respectively.

These viscosities and those of Bair *(21)* were fitted to the improved Yasutomi model (Eqs. [3]–[5]) with $\mu_g = 1.23 \times 10^7$ Pa·s. The resulting parameters are listed in Table 3 and T_g extrapolated to ambient pressure is found to be 184.5 K, 10 K greater than that from the hot-wire measurement. The viscosities are compared with the model in Fig. 4. The standard devia-

Table 1. Glass transition temperature at elevated pressures from transient hot-wire. T_g corresponds to a heat capacity relaxation time of about 0.3 s.

p (GPa)	T_g (K)
0.0001	174.4
0.025	178
0.075	185
0.15	194
0.25	206
0.35	217
0.45	227
0.6	238
0.8	256.2

Table 3. Parameters of the improved Yasutomi model.

Parameter	Squalane	SQL + PIP
μ_g (Pa·s)	1.23×10^7	1×10^{12}
T_{g0} (°C)	−88.69	−73.62
A_1 (°C)	263.8	554.1
A_2 (GPa^{-1})	0.3527	0.0933
b_1 (GPa^{-1})	13.73	8.39
b_2	−0.3426	−0.5300
C_1	11.66	15.49
C_2 (°C)	39.17	20.12
SD (%)	9.2	2.6

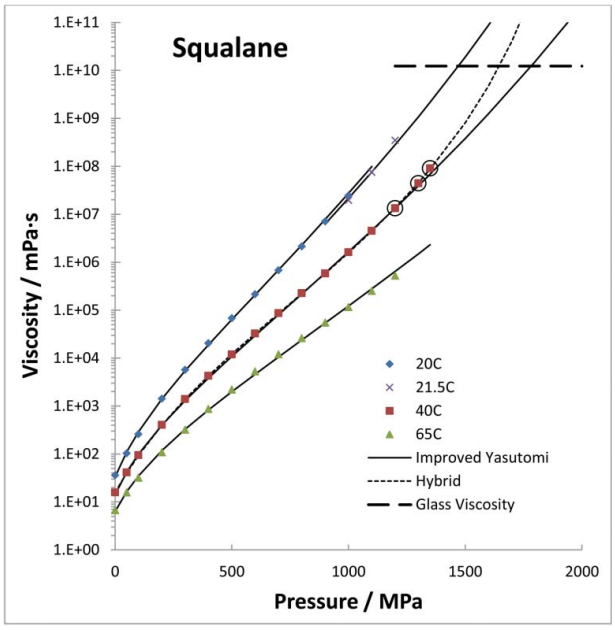

Figure 4. Measured viscosity of squalane from Bair, et al. *(11)* and this work. The improved Yasutomi model and the hybrid model with newly regressed parameters are shown. The new data at 40°C are circled. All at 21.5°C are new.

tion of 9% is actually good for any correlation for temperature and pressure of data spanning eight orders of magnitude. The glass transition temperatures from the hot wire are plotted in Fig. 5 and compared with the Oels and Rehage *(29)* equation fitted to these hot-wire data and the same equation derived from the viscosity. Notice in Fig. 4 that the improved Yasutomi model (Eq. [3]) does not fully account for the upturn in viscosity for the highest pressures at 21.5 and 40°C. This is a common issue for pressure–viscosity correlations, which will be discussed below. If the model curves were to turn upward faster, they would reach the glass viscosity at lower pressure and this would likely provide better agreement with the pressure dependence of the measured glass temperatures in Fig. 5.

Richert, et al. *(41)* defined T_g as the temperature at which the primary dielectric relaxation time was $\lambda_{diel} = 100$ s. From a VTF fit to their dielectric relaxation time measurements of squalane, $T_g = 167.4$ K at ambient pressure. Then from the Deegan, et al. *(39)* VTF fit to viscosity, $\mu_g = 8.5 \times 10^8$ Pa·s and $\mu/\lambda_{diel} = 8.5$ MPa, a typical value for oils at ambient pressure.

A correlation is required in an EHL simulation to describe, at the least, the pressure dependence of the viscosity of the liquid and, often, the temperature dependence as well. After choosing a property relation that, hopefully, is capable of reproducing all of the trends in the data, a regression analysis is used to find the parameters of the correlation that reduces some measure of the deviations. This approach is helpful in some applications; however, in EHL the sensitivity of the viscosity to pressure, $\partial \ln\mu/\partial p$, is important, too. The pressure–viscosity slope near $p = 0$ influences the film thickness and the pressure–viscosity slope at the maximum contact pressure influences the slope of the logarithmic portion of the friction curve (Bair, et al. *(6)*). Unfortunately, the $\partial \ln\mu/\partial p$ that exists in the data is not weighted in the usual regression analysis. This can be shown in Fig. 6, which is a pressure–Stickel plot (Casalini, et al. *(42)*) of $[\partial \ln(\mu)/\partial p]^{-1/2}$ versus pressure for squalane at 40°C. In this presentation, the Paluch equation (Paluch, et al. *(43)*),

$$\mu = \mu_0 \exp\left(\frac{C_F p}{p_\infty - p}\right), \qquad [6]$$

plots as a descending straight line.

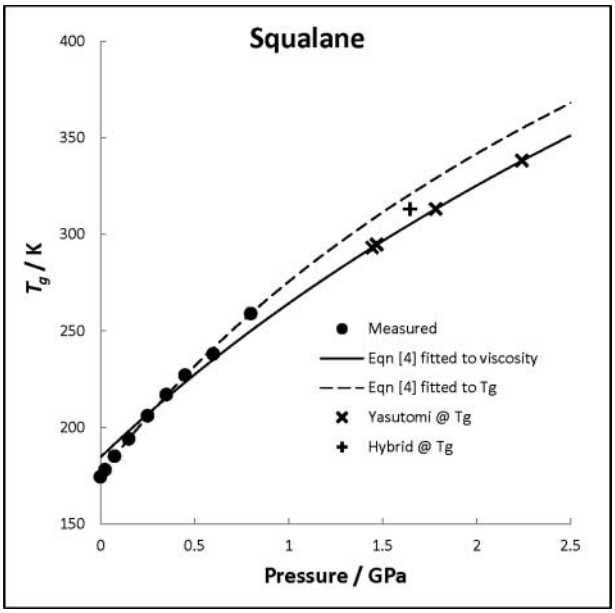

Figure 5. Glass transition temperature as a function of pressure. Circles represent the transition detected in the thermal properties and correspond to a relaxation time of about 0.3 s. The × s represent the pressures at which the improved Yasutomi viscosity reaches μ_g. The + represents the pressure at which the hybrid model viscosity reaches μ_g.

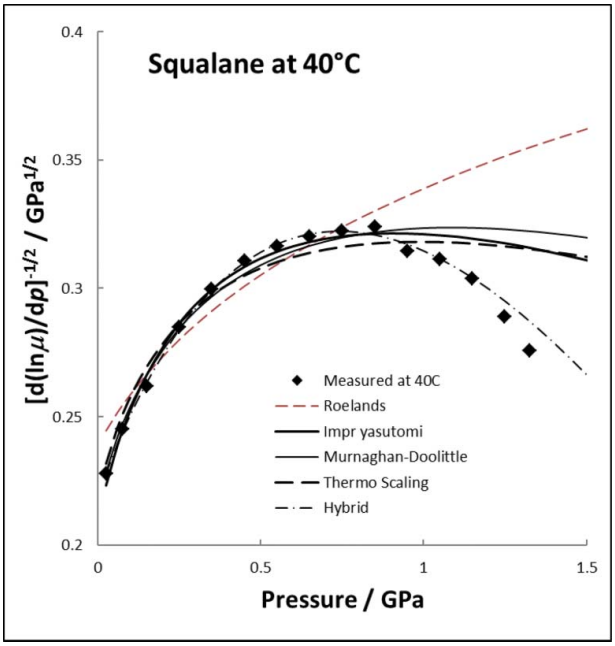

Figure 6. A pressure–Stickel plot (Giordano, et al. *(35)*) of $[\partial \ln(\mu)/\partial p]^{-1/2}$ versus pressure for squalane at 40°C. The various curves represent correlations that have been applied to the data of Bair, et al. *(11)*, which extend to only 1.2 GPa. The points were calculated from those data and the two new viscosities at 1.3 and 1.35 GPa presented here as represented by the two points at the highest pressures.

Table 4. Parameters of the hybrid model for data to $p = 1{,}350$ and to 1,200 MPa.

	Squalane	Squalane
Temperature (°C)	40	40
Pressure (MPa)	0.1 to 1,350	0.1 to 1,200
μ_0 (mPa·s)	0.0158	0.01566
α_0 (GPa^{-1})	18.03	17.836
q	5.324	4.412
C_F	5.515	8.923
p_∞ (GPa)	2.517	3.030
SD (%)	2.0	0.7

The various curves in Fig. 6 represent correlations that have been applied to the data of Bair *(21)* at 40°C that extend to only 1.2 GPa. The points are calculated from those data and the two highest pressure entries represent the new viscosities at 1.3 and 1.35 GPa. The correlations are the improved Yasutomi (Bair, et al. *(31)*), the Murnghan-Doolittle free volume (Bair *(21)*), the Vogel-like thermodynamic scaling (Björling, et al. *(10)*), and the hybrid model (Bair *(44)*),

$$\mu = \mu_0 \left(1 + \frac{\alpha_0}{q} p\right)^q \exp\left(\frac{C_F p}{p_\infty - p}\right), \qquad [7]$$

which combines the faster-than-exponential response of the Paluch equation (Eq. [6]) at high pressure with the slower-than-exponential behavior of the McEwen equation (McEwen *(45)*). The Roelands model has also been fitted to the data to 1.2 GPa. This is the most widely used expression in classical EHL, although it is inappropriate for the task. Clearly, the hybrid model is best for extrapolation, and in Fig. 5 the pressure at the glass viscosity is a better fit to the measured glass temperatures. Adding the new data to those already available for squalane at 40°C, the parameters of the hybrid model have been newly regressed and are listed in Table 4 for pressures to 1.2 GPa and again for 1.35 GPa. The hybrid model is plotted in Fig. 4 with the new parameters.

The characteristic time of an EHL contact might be regarded as the transit time through the high-pressure region. For example, if the contact width is 2×10^{-4} m and the speed is 0.01 to 5 m/s, then the characteristic time is 2×10^{-2} to 4×10^{-5} s or 15 to 7,500 times less than that of the hot-wire experiment. This would make the glass transition viscosity 15 to 7,500 times lower than 10^7 Pa·s or as low as 10^3 Pa·s in some cases. If squalane were to take on solid-like thermophysical properties at pressures that yield such low viscosity, the friction response might be expected to be much different from calculations based upon measurements with long characteristic times. Comparing the deviations in friction for the high- and low-pressure cases of Björling, et al. *(10)*, the effect is not apparent.

Squalane + Polyisoprene shear-dependent viscosity

Before exploring the shear thinning of SQL + PIP, the existing low-shear viscosity data to 1.0 GPa from Bair *(21)* were fitted to the improved Yasutomi model (Eqs. [3]–[5]) and the parameters are entered in Table 3. The universal value of $\mu_g = 10^{12}$ Pa·s was retained here.

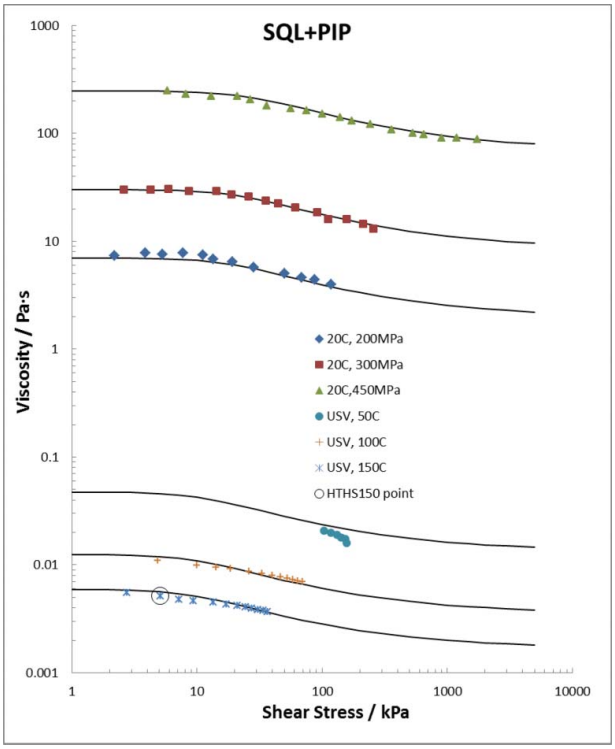

Figure 7. Steady shear viscosity of squalane plus 15% polyisoprene with new data at ambient pressure. The data at 50, 100, and 150°C are new. Cavitation appears at ambient pressure for shear stress greater than 60 kPa. Time–temperature–pressure superposition applies.

Existing shear-dependent data (Bair *(21)*, *(46)*) are plotted in Fig. 7 for 200, 300, and 450 MPa, the three upper flow curves. New high-shear rate data at ambient pressure were generated with an ultrashear viscometer. These are the three lower flow curves for 50, 100, and 150°C. The high-temperature, high-shear at 150°C condition (HTHS150) is indicated by a circle on the plots where the shear rate is 10^6 s^{-1}. The shear stress for the HTHS150 condition is 5 kPa for which the viscosity is 5.11 mPa·s compared to the limiting low-shear value of 6.09 mPa·s. The HTHS150 condition is not sufficiently severe to greatly shear-thin this oil.

Shear thinning occurs when the product of shear rate (or frequency) and the rotational relaxation time of a molecule approaches unity. This relaxation time is approximately proportional to the low-shear viscosity. Hence, the product of shear rate and viscosity, the shear stress, is approximately constant at the Newtonian limit. The presentation of Fig. 7, viscosity as a function of shear stress, illustrates this superposition property of shear-thinning liquids. Flow curves can be superimposed by a vertical shift long a path of nearly constant shear stress. The exception is the data at ambient pressure and 50°C.

The failure of the measurement to superimpose at ambient pressure and 50°C is due to shear cavitation in which a tensile stress appears in one of the principal shear stress directions (Kottke, et al. *(47)*). The principal normal

stress cavitation criterion predicts that the first cavitation bubbles appear when (Kottke, et al. *(47)*),

$$\frac{N_1+\sqrt{N_1{}^2+4\tau^2}}{2}>p, \qquad [8]$$

where N_1 is the primary normal stress difference, the tensile stress in the flow direction less the tensile stress in the cross-flow direction. For polymer-thickened oils, N_1 may be estimated from (Bair *(48)*):

$$N_1=\frac{2\tau^2}{G}, \qquad [9]$$

where G is the Newtonian limit shear stress obtained from a measurement of shear thinning.

The curves in Fig. 7 are the modified Carreau equation (Habchi, et al. *(7)*).

$$\eta=\mu_2+(\mu-\mu_2)\left[1+\left(\frac{\tau}{G}\right)^2\right]^{\frac{1-\frac{1}{n}}{2}}. \qquad [10]$$

The shifting rule is

$$G=G_R\left(\frac{\mu}{\mu_R}\right)^m, \qquad [11]$$

with $n=$ 0.65, $\mu_2/\mu=$ 0.28, $G_R=$ 19 kPa, $\mu_R=$ 10 Pa·s, and $m=$ 0.1 obtained by fitting the flow curves. The value of m is typical. The principal normal stress cavitation criterion predicts cavitation bubbles at ambient pressure for shear stress greater than 23 kPa.

The solvent, in this case squalane, begins to shear-thin as the shear stress approaches 6 MPa (Bair *(13)*), at the termination of the curves plotted in Fig. 7. Shear thinning of the base oil usually precludes a second Newtonian plateau in gear oils as it would here.

Generally, steady shear viscosity measurements at ambient pressure cannot sustain sufficient shear stress due to cavitation to observe the second Newtonian inflection in modern lubricants, much less reach any second Newtonian plateau. However, oscillatory shear measurements can produce shear thinning without generating high shear stress (Bair, et al. *(49)*), as demonstrated in the following.

Squalane + Polyisoprene viscosity at high frequency

The viscosity of SQL + PIP was measured at atmospheric pressure using a calibrated acoustic viscometer based on matching layer theory (Schirru, et al. *(50)*). Ultrasonic viscometers shear the fluid by exciting the vibration of the solid–fluid boundary, using polarized acoustic shear waves. A shear ultrasonic wave that is incident to a liquid is partly transmitted (and quickly dissipated) in the liquid and partly reflected. The amount of energy that is reflected is a function of viscosity. Ordinarily, the acoustic impedance of the solid is much higher than the liquid impedance, giving a reflection coefficient close to unity and, therefore, insensitive to the viscosity. The use of an interposed matching material, a 40-μm-thick polyimide layer, between the solid and the oil overcomes the acoustic mismatch and increases the sensitivity to viscosity (Schirru and Dwyer-Joyce *(51)*).

Table 5. Viscosity of SQL + PIP by ultrasonic reflection at ambient pressure.

Frequency (MHz)	Temperature (°C)	Reflection coefficient	Viscosity (mPa·s)
1	23	0.8915	84.0
5	25	0.7612	55.2
15	25	0.5490	52.8

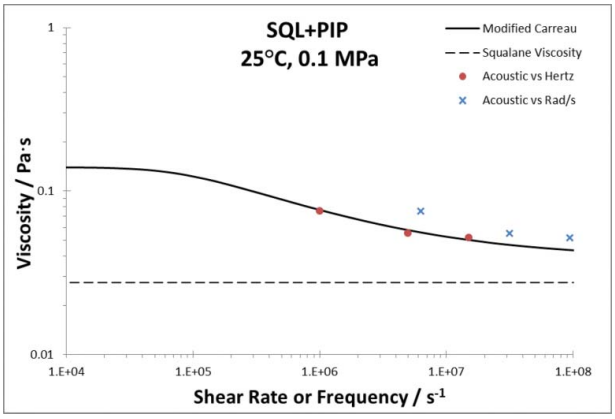

Figure 8. Viscosity from the acoustic viscometer as a function of frequencies compared with the modified Carreau equation shifted to ambient pressure at 25°C.

The ultrasonic reflection from the sample was converted to viscosity using a viscoelastic semi-empirical Maxwell model (Schirru, et al. *(50)*; Schirru and Dwyer-Joyce *(51)*). It was possible to excite fluid resonance at 1, 5, and 15 MHz, resulting in the viscosities listed in Table 5. The 1 MHz viscosity at 23°C, 84.0 mPa·s, can be used to estimate the 1 MHz viscosity, 75.7 mPa·s, at 25°C using the temperature dependence from the improved Yasutomi correlation. These viscosities at 25°C are plotted in Fig. 8 as a function of frequency. Two definitions for frequency are used. Normal frequency, f (Hz), is the reciprocal of the period of the oscillation and angular frequency is $\omega=2\pi f$ (rad/s).

The Cox-Merz rule provides an analogy between the viscosities in steady and oscillatory shear (Bair, et al. *(49)*):

$$\eta(\dot\gamma)=\hat\eta(\omega),\quad \dot\gamma=\omega. \qquad [12]$$

This rule may be tested with the shifted modified Carreau equation [10], which is the curve plotted in Fig. 8. Clearly the steady and oscillatory analogy for this viscometer comes with equating ordinary frequency with shear rate:

$$\eta(\dot\gamma)=\hat\eta(f),\quad \dot\gamma=f \qquad [13]$$

and the agreement is good. Notably, the viscosity generated by the acoustic technique with matching layer does define the second Newtonian inflection for ambient pressure in SQL + PIP, whereas steady shear cannot.

Conclusions

1. The glass transition viscosity of squalane at ambient pressure was found from published viscosity measurements and new glass transition measurements by transient hot-wire for a characteristic time of 0.3 s.
2. The glass transition viscosity was incorporated into the improved Yasutomi model and the calculated glass temperatures as a function of pressure are comparable to those directly measured, although the hybrid model yields better agreement.
3. The hybrid model is superior to many others for pressure extrapolation.
4. The glass transition viscosity of squalane by any definition must be substantially lower than the universal value of 10^{12} Pa·s.
5. The second Newtonian inflection cannot be characterized in steady shear at ambient pressure for SQL + PIP due to cavitation.
6. The shear stress at the HTHS150 condition is insufficient to characterize the shear dependence of SQL + PIP.
7. Acoustic viscometry with a matching layer does characterize the second Newtonian inflection for SQL + PIP.
8. To form the analogy between steady and oscillatory shear requires that the steady shear rate be compared with the ordinary frequency rather than the angular frequency for SQL + PIP.

Acknowledgement

Bair thanks Mark Robbins of Johns Hopkins for suggesting the additional viscosity measurements of squalane.

References

(1) Holzapfel, W. B. and Isaacs, N. S. (1997), *High Pressure Techniques in Chemistry and Physics—A Practical Approach*, New York, NY: Oxford University Press.
(2) Hayward, A. T. J. (1967), "Compressibility Equations for Liquids: A Comparative Study," *British Journal of Applied Physics*, **18**(7), pp 965–977.
(3) Hutton, J. F. and Phillips, M. C. (1973), "High Pressure Viscosity of a Polyphenyl Ether Measured with a New Couette Viscometer," *Nature*, **245**(140), pp 15–16.
(4) Bair, S. (2015), "A Critical Evaluation of Film Thickness−Derived Pressure–Viscosity Coefficients," *Lubrication Science*, **27**(6), pp 337–346.
(5) Bair, S., Vergne, P., Kumar, P., Poll, G., Krupka, I., Hartl, M., Habchi, W., and Larsson, R. (2015), "Comment on 'History, Origins and Prediction of Elastohydrodynamic Friction' by Spikes and Jie," *Tribology Letters*, **58**(1), pp 1–8.
(6) Bair, S., Martinie, L., and Vergne, P. (2016), "Classical EHL versus Quantitative EHL: A Perspective Part II—Super-Arrhenius Piezoviscosity, an Essential Component of Elastohydrodynamic Friction Missing from Classical EHL," *Tribology Letters*, **63**(3).
(7) Habchi, W., Bair, S., Qureshi, F., and Covitch, M. (2013), "A Film Thickness Correction Formula for Double-Newtonian Shear-Thinning in Rolling EHL Circular Contacts," *Tribology Letters*, **50**(1), pp 59–66.
(8) Ree, F., Ree, T., and Eyring, H. (1958), "Relaxation Theory of Transport Problems in Condensed Systems," *Industrial & Engineering Chemistry*, **50**(7), pp 1036–1040.
(9) Johnson, K. L. and Tevaarwerk, J. L. (1977), "Shear Behaviour of Elastohydrodynamic Oil Films," *Proceedings of the Royal Society of London A: Mathematical, Physical and Engineering Sciences*, **356** (1685), pp 215–236.
(10) Björling, M., Habchi, W., Bair, S., Larsson, R., and Marklund, P. (2013), "Towards the True Prediction of EHL Friction," *Tribology International*, **66**, pp 19–26.
(11) Bair, S., Roland, C. M., and Casalini, R. (2007), "Fragility and the Dynamic Crossover in Lubricants," *Proceedings of the Institution of Mechanical Engineers - Part J: Journal of Engineering Tribology*, **221** (7), pp 801–811.
(12) Bair, S., Fernandez, J., Khonsari, M. M., Krupka, I., Qureshi, F., Vergne, P., and Wang, Q. J. (2009), "Letter to the Editor: An Argument for a Change in the Philosophy of Elastohydrodynamic Lubrication," *Proceedings of the Institution of Mechanical Engineers - Part J: Journal of Engineering Tribology*, **223**(4), pp i–ii.
(13) Bair, S. (2002), "The High Pressure Rheology of Some Simple Model Hydrocarbons," *Proceedings of the Institution of Mechanical Engineers - Part J: Journal of Engineering Tribology*, **216**(3), pp 139–149.
(14) Liu, Y., Wang, Q. J., Wang, W., Hu, Y., Zhu, D., Krupka, I., and Hartl, M. (2006), "EHL Simulation Using the Free-Volume Viscosity Model," *Tribology Letters*, **23**(1), pp 27–37.
(15) Johnston, G. J., Wayte, R., and Spikes, H. A. (1991), "The Measurement and Study of Very Thin Lubricant Films in Concentrated Contacts," *Tribology Transactions*, **34**(2), pp 187–194.
(16) Liu, Y., Wang, Q. J., Bair, S., and Vergne, P. (2007), "A Quantitative Solution for the Full Shear-Thinning EHL Point Contact Problem Including Traction," *Tribology Letters*, **28**(2), pp 171–181.
(17) Krupka, I., Bair, S., Kumar, P., Khonsari, M. M., and Hartl, M. (2009), "An Experimental Validation of the Recently Discovered Scale Effect in Generalized Newtonian EHL," *Tribology Letters*, **33** (2), pp 127–135.
(18) Krupka, I., Kumar, P., Bair, S., Khonsari, M. M., and Hartl, M. (2010), "The Effect of Load (Pressure) for Quantitative EHL Film Thickness," *Tribology Letters*, **37**(3), pp 613–622.
(19) Habchi, W., Vergne, P., Bair, S., Andersson, O., Eyheramendy, D., and Morales-Espejel, G. E. (2010), "Influence of Pressure and Temperature Dependence of Thermal Properties of a Lubricant on the Behaviour of Circular TEHD Contacts," *Tribology International*, **43** (10), pp 1842–1850.
(20) Sax, K. J. and Stross, F. H. (1957), "Squalane: A Standard," *Analytical Chemistry*, **29**(11), pp 1700–1702.
(21) Bair, S. (2006), "Reference Liquids for Quantitative Elastohydrodynamics: Selection and Rheological Characterization," *Tribology Letters*, **22**(2), pp 197–206.
(22) Harris, K. R. (2009), "Temperature and Pressure Dependence of the Viscosities of 2-Ethylhexyl Benzoate, Bis (2-Ethylhexyl) Phthalate, 2,6,10,15,19,23-Hexamethyltetracosane (Squalane), and Diisodecyl Phthalate," *Journal of Chemical & Engineering Data*, **54**(9), pp 2729–2738.
(23) Pensado, A. S., Comunas, M. J. P., Lugo, L., and Fernández, J. (2006), "High-Pressure Characterization of Dynamic Viscosity and Derived Properties for Squalane and Two Pentaerythritol Ester Lubricants: Pentaerythritol Tetra-2-Ethylhexanoate and Pentaerythritol Tetrananoate," *Industrial & Engineering Chemistry Research*, **45**(7), pp 2394–2404.
(24) Fandino, O., Pensado, A. S., Lugo, L., Comunas, M. J. P., and Fernández, J. (2005), "Compressed Liquid Densities of Squalane and Pentaerythritol Tetra (2-Ethylhexanoate)," *Journal of Chemical & Engineering Data*, **50**(3), pp 939–946.
(25) Comuñas, M. J., Paredes, X., Gaciño, F. M., Fernández, J., Bazile, J. P., Boned, C., and Harris, K. R. (2014), "Viscosity Measurements for Squalane at High Pressures to 350 MPa from $T =$ (293.15 to 363.15) K," *The Journal of Chemical Thermodynamics*, **69**, pp 201–208.
(26) Williams, M. L., Landel, R. F., and Ferry, J. D. (1955), "The Temperature Dependence of Relaxation Mechanisms in Amorphous Polymers and Other Glass-Forming Liquids," *Journal of the American Chemical Society*, **77**(14), pp 3701–3707.
(27) Angell, C. A. (1995), "Formation of Glasses from Liquids and Biopolymers," *Science*, **267**(5206), pp 1924–1935.
(28) Yasutomi, S., Bair, S., and Winer, W. O. (1984), "An Application of a Free Volume Model to Lubricant Rheology I—Dependence of

Viscosity on Temperature and Pressure," *Journal of Tribology*, **106** (2), pp 291–302.

(29) Oels, H. J. and Rehage, G. (1977), "Pressure–Volume–Temperature Measurements on Atactic Polystyrene. A Thermodynamic View," *Macromolecules*, **10**(5), pp 1036–1043.

(30) Weitz, A. and Wunderlich, B. (1974), "Thermal Analysis and Dilatometry of Glasses Formed under Elevated Pressure," *Journal of Polymer Science: Polymer Physics Edition*, **12**(12), pp 2473–2491.

(31) Bair, S., Mary, C., Bouscharain, N., and Vergne, P. (2013), "An Improved Yasutomi Correlation for Viscosity at High Pressure," *Proceedings of the Institution of Mechanical Engineers - Part J: Journal of Engineering Tribology*, **227**, pp 1056–1060.

(32) Håkansson, B., Andersson, P., and Bäckström, G. (1988), "Improved Hot−Wire Procedure for Thermophysical Measurements under Pressure," *Review of Scientific Instruments*, **59**(10), pp 2269–2275.

(33) Andersson, O. (1997), "Simulation of a Glass Transition in a Hot-Wire Experiment Using Time-Dependent Heat Capacity," *International Journal of Thermophysics*, **18**(1), pp 195–208.

(34) Matusita, K., Koide, M., and Komatsu, T. (1992), "Viscosity of Fluoride Glasses at Glass Transition Temperature," *Journal of Non-Crystalline Solids*, **140**, pp 119–122.

(35) Giordano, D., Nichols, A. R., and Dingwell, D. B. (2005), "Glass Transition Temperatures of Natural Hydrous Melts: A Relationship with Shear Viscosity and Implications for the Welding Process," *Journal of Volcanology and Geothermal Research*, **142**(1), pp 105–118.

(36) Schweyer, H. E. (1974), "Glass Transition of Asphalts under Pressure," *Journal of Testing and Evaluation*, **2**(1), pp 50–56.

(37) Bair, S. (1993), "An Experimental Verification of the Significance of the Reciprocal Asymptotic Isoviscous Pressure for EHD Lubricants," *Tribology Transactions*, **36**(2), pp 153–162.

(38) Alsaad, M. S. D. M., Bair, S., Sanborn, D. M., and Winer, W. O. (1978), "Glass Transitions in Lubricants: Its Relation to Elastohydrodynamic Lubrication (EHD)," *Journal of Lubrication Technology*, **100**(3), pp 404–416.

(39) Deegan, R. D., Leheny, R. L., Menon, N., Nagel, S. R., and Venerus, D. C. (1999), "Dynamic Shear Modulus of Tricresyl Phosphate and Squalane," *Journal of Physical Chemistry B*, **103**(20), pp 4066–4070.

(40) Bair, S. (2000), "Pressure–Viscosity Behavior of Lubricants to 1.4 GPa and Its Relation to EHD Traction," *Tribology Transactions*, **43**(1), pp 91–99.

(41) Richert, R., Duvvuri, K., and Duong, L. T. (2003), "Dynamics of Glass-Forming Liquids. VII. Dielectric Relaxation of Supercooled Tris-Naphthylbenzene, Squalane, and Decahydroisoquinoline," *Journal of Chemical Physics*, **118**(4), pp 1828–1836.

(42) Casalini, R., Paluch, M., and Roland, C. M. (2003), "Dynamic Crossover in Supercooled Liquids Induced by High Pressure," *Journal of Chemical Physics*, **118**(13), pp 5701–5703.

(43) Paluch, M., Dendzik, Z., and Rzoska, S. J. (1999), "Scaling of High-Pressure Viscosity Data in Low-Molecular-Weight Glass-Forming Liquids," *Physical Review B*, **60**(5), pp 2979–2982.

(44) Bair, S. (2015), "Choosing Pressure–Viscosity Relations," *High Temperatures–High Pressures*, **44**(6), pp 415–428.

(45) McEwen, E. (1952), "The Effect of Variation of Viscosity with Pressure on the Load-Carrying Capacity of the Oil Film between Gear-Teeth," *Journal of the Institute of Petroleum*, **38**(344–345), pp 646–672.

(46) Bair, S. (2009), "Rheology and High-Pressure Models for Quantitative Elastohydrodynamics," *Proceedings of the Institution of Mechanical Engineers - Part J: Journal of Engineering Tribology*, **223**(4), pp 617–628.

(47) Kottke, P. A., Bair, S. S., and Winer, W. O. (2005), "Cavitation in Creeping Shear Flows," *AIChE Journal*, **51**(8), pp 2150–2170.

(48) Bair, S. (2015), "The First Normal Stress Difference in a Shear-Thinning Motor Oil at Elevated Pressure," *Tribology Transactions*, **58**(4), pp 654–659.

(49) Bair, S., Yamaguchi, T., Brouwer, L., Schwarze, H., Vergne, P., and Poll, G. (2014), "Oscillatory and Steady Shear Viscosity: The Cox-Merz Rule, Superposition, and Application to EHL Friction," *Tribology International*, **79**, pp 126–131.

(50) Schirru, M., Mills, R., Dwyer-Joyce, R., Smith, O., and Sutton, M. (2015), "Viscosity Measurement in a Lubricant Film Using an Ultrasonically Resonating Matching Layer," *Tribology Letters*, **60**(3), pp 1–11.

(51) Schirru, M. M. and Dwyer-Joyce, R. S. (2016), "A Model for the Reflection of Shear Ultrasonic Waves at a Thin Liquid Film and Its Application to Viscometry in a Journal Bearing," *Proceedings of the Institution of Mechanical Engineers - Part J: Journal of Engineering Tribology*, **230**(6), pp 667–679.